DOI:
10.1016/j.ces.2022.118159

Document Version
Publisher's PDF, also known as Version of record

Chemical Engineering Science 264 (2022) 118159

Contents lists available at ScienceDirect

Chemical Engineering Science

journal homepage: www.elsevier.com/locate/ces

Synthesis and ^{68}Ga radiolabelling of calcium alginate beads for positron emission particle tracking (PEPT) applications

Juan Pellico [a,*], Ananda Jadhav [b], Laurence Vass [a], Agathe Bricout [a], Mostafa Barigou [b], Paul K. Marsden [a], Rafael T.M. de Rosales [a,*]

[a] School of Biomedical Engineering & Imaging Sciences, King's College London, St. Thomas' Hospital, London SE1 7EH, United Kingdom
[b] School of Chemical Engineering, University of Birmingham, Edgbaston, Birmingham B15 2TT, United Kingdom

HIGHLIGHTS

- Calcium alginate beads with different particle size, specific surface, concentration, and composition were synthesised for application as PEPT tracers.
- Simple and efficient radiolabelling of alginate beads with ^{68}Ga, a generator-produced radionuclide.
- Excellent radiochemical properties regardless of the number of beads, the concentration of alginate, their size, or the composition of the beads.
- High performance in PEPT phantom demonstrates the ability to track cubic trajectories.
- First ^{68}Ga-radiolabelled material for applications in PEPT.

ARTICLE INFO

Article history:
Received 25 July 2022
Received in revised form 21 September 2022
Accepted 28 September 2022
Available online 4 October 2022

Keywords:
PEPT
Calcium Alginate beads
Ga-68
Radiolabelled materials
Preclinical scanner

ABSTRACT

Positron emission particle tracking (PEPT) relies on the back-to-back γ-rays generated through a positron annihilation to track a single radiolabelled particle in three dimensions and in dense, multiphase, and opaque systems. The spectrum of applications of PEPT such as batch mixing systems in chemical, food and pharmaceutical sectors or granulation, die-filling and fluidisation in industrial processes, is directly related to the development of efficient radiolabelled materials and often restricted due to the lack of suitable materials with adequate radiochemical properties. In this work, we report a straightforward synthesis and radiolabelling of calcium alginate beads of different size, specific surface, concentration, and density, with the positron emitter gallium-68 (^{68}Ga) to cover a broad range of possibilities in PEPT. We demonstrate a high intrinsic affinity between alginate and ^{68}Ga providing directly radiolabelled particles with excellent radiochemical properties and excellent performance for tracking complex trajectories. These results, in combination with the availability and relatively simple chemistry of ^{68}Ga, provide a high versatile and straightforward platform for the future development and advance of PEPT in different applications.

1. Introduction

Particle-fluid flows in pipes, vessels and microchannels is a generic complex problem with applications across medicine and diverse industries ranging from blood flow to food and pharmaceutical processing, through chemical, consumer goods, oil, mining, construction, river engineering and power generation industries (Cole et al., 2022; Tripathi and Vasu, 2021; Barigou and Muller, 2015; Başağaoğlu et al., 2013; Siddiqui and Turkyilmazoglu, 2019; Siddiqui and Turkyilmazoglu, 2020). Despite the large range of application areas, particle-liquid flow science is still far from optimal for industrial processes and clinical practice due to a severe lack of fundamental understanding. This problem is particularly challenging when investigating dense, multiphase, opaque systems. A relatively unexplored technique to study flow phenomena in such systems is positron emission particle tracking (PEPT) (Windows-Yule et al., 2022; Sommer et al., 2020; Hoffmann et al., 2019). PEPT involves measurement of the motion of a moving positron-emitting radiolabelled particulate tracer within a system of flow (Cole et al., 2014). PEPT relies on tracking single particles (tracers) within a bulk fluid in the system. These tracers need to carry enough radioactivity for detection (5–10 MBq/particle) and be capable of withstanding the conditions of the intended application (*e.g.* resistance to abrasion, chemical, physical and radiochem-

* Corresponding authors.
E-mail addresses: juan.pellico@kcl.ac.uk (J. Pellico), rafael.torres@kcl.ac.uk (R. T.M. de Rosales).

https://doi.org/10.1016/j.ces.2022.118159
0009-2509/

ical stability in water/other fluids) (Windows-Yule et al., 2020). In addition, to reflect the behaviour of the fluid of interest, the tracer material is required to be near-identical to the bulk.

Previous PEPT tracers involved particles of high density materials such as alumina or silica that were radiolabelled by direct activation in a cyclotron to induce the ^{16}O (^{3}H, p)^{18}F reaction, producing ^{18}F-labelled particles (Parker and Fan, 2008). This strategy can provide efficient radiolabelling for materials between 1 and 10 mm but is limited to materials that are stable at high temperatures. Furthermore, the high density of these particles is usually not appropriate for the purpose (Fan et al., 2006). Other strategies have explored the indirect radiolabelling of smaller particles, based on granulated anion exchange resins, by mixing an aqueous $^{18}F^-$ solution with a suspension of particles and further isolation (Parker and Fan, 2008). Although this strategy provides radiolabelled particles with suitable densities and sizes, it results in low radiochemical stabilities (RCS) in water. A high RCS is mandatory in PEPT studies as the presence of non-attached "free" radionuclide can provide misleading results (tracking of free radionuclide).

To overcome the limitations of current PEPT tracers described above, in this work we explored the use of beads made of calcium alginate ($(C_{12}H_{14}CaO_{12})_n$) and radiolabelled with Ga-68 as efficient PEPT tracers. Alginate is a natural polysaccharide derived from brown seaweed and its basic structure consists of linear binary copolymers of 1 → 4 linked α-D-mannuronic acid (M block) and β-L-guluronic acid (G block) (Fig. 1). It forms thermally stable and biocompatible hydrogel beads in the presence of calcium ions. Calcium alginate beads are widely used for encapsulation of microbial cells, enzymes, hormones, drugs, oils, herbal extracts, and flavours (Lee et al., 2013). We hypothesised that calcium alginate particles should have an intrinsic affinity for metallic positron emitters such as Ga-68 as well as the possibility of modulation of important properties such as concentration, porosity, size, and density providing excellent tracers for a wide range of PEPT applications.

Gallium-68 (^{68}Ga, $t_{1/2}$ = 67.71 min) (McCutchan, 2012) is a positron emitter radionuclide, mainly used for the radiolabelling of peptides and small molecules (Shetty et al., 2010; Banerjee and Pomper, 2013). The main advantage of this radionuclide is its availability from clinical-grade $^{68}Ge/^{68}Ga$ benchtop generators that avoids the necessity of on site large and costly facilities such as cyclotrons. Radiolabelling with $^{68}Ga^{3+}$ ions is usually based on the use of chelating ligands possessing carboxyl, phosphonic, hydroxyl or amine donor groups (Blower et al., 2021). In this work, the high affinity of ^{68}Ga for carboxyl donor groups was exploited for the direct radiolabelling of the alginate beads. The hypothesis relies on the presence of high numbers of carboxyl and hydroxyl donor groups in the alginate structure, to provide stable coordination complexes with ^{68}Ga and leading to a single straightforward reaction protocol under mild conditions. Several important parameters of this reaction, such as the number, porosity, and size of beads as well as the modification in the alginate concentration and composition were evaluated providing a comprehensive study of these new class of PEPT radiotracers. In addition, their suitability for PEPT applications was tested using a preclinical PET scanner. This work represents not only the first reported synthesis of a suitable material with modulated properties by a single step synthesis but the first reported example of a ^{68}Ga radiolabelled particle for PEPT.

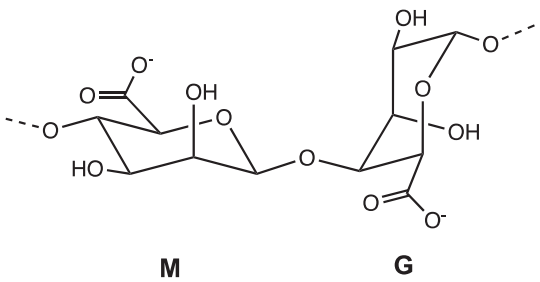

Fig. 1. Chemical structure of alginate.

2. Materials and methods

Synthesis of alginate beads 4 %(w/w) (CABs). In a typical calcium alginate bead preparation, two separate 100 mL solutions, one containing 4 % (w/w) of sodium alginate (Sigma-Aldrich Company ltd, UK) and the other 4 % (w/w) of calcium chloride (Scientific Laboratory Supplies ltd, UK), were prepared in pure water. The sodium alginate solution was then slowly dripped through a stainless-steel needle into the calcium chloride solution using a peristaltic pump under gentle stirring. The calcium alginate beads of size 4, 8 and 10 mm were produced using needles/capillary of inner diameter of 2 mm, 4.1 mm, and 5.2 mm, respectively and the shape was controlled by keeping the distance between the edge of the needle and the surface of the calcium solution at 60 cm, as schematically represented in Fig. 3(A). The stirring was continued for one hour to ensure complete cross-linking. After that the calcium alginate beads were harvested by filtration, washed with distilled water, and stored in pure water in an airtight container. For the alginate beads at 10 %(w/w), the initial concentrations of sodium alginate and calcium chloride were increased for 4 % to 10 %(w/w) Table 1.

Note that the minimum and maximum concentration of sodium alginate solution for the synthesis of calcium alginate beads used is 4 and 10 w/w%, respectively. Beads prepared with<4 w/w% are extremely soft and disintegrate when sheared, and above 10 w/w % the sodium alginate solution becomes very viscous and difficult to produce by extrusion dripping. Furthermore, for this study, we prepared and used calcium alginate beads with diameters ranging from 4 to 10 mm because this coarse size is relevant to several industrial applications.

Synthesis of alginate beads 10 %(w/w) with ultrasounds (10 % US). Using a similar setup to that described above, calcium alginate with increased specific surface were prepared by adding the sodium alginate to calcium chloride solution under ultrasonic irradiation (Elmasonic P180H Ultrasonic, UK) instead of using a magnetic stirrer, as schematically represented in Fig. 3(B). The cavitation was carried out at room temperature using 37 kHz frequency.

Synthesis of silica encapsulated calcium alginate beads (CASiBs). Silica encapsulated calcium alginate beads were prepared as described above. In this case a 10 % (w/w) of silica powder (Warm Glass, UK) was added to the sodium alginate solution prior to the reaction. The mixture of silica and sodium alginate was continuously stirred during the calcium alginate preparation process to ensure homogeneity. For purification, silica-encapsulated calcium alginate beads were collected by filtration, washed with distilled water to remove the free (nonencapsulated) silica, and stored in pure water in an airtight container.

Synthesis of polyvinyl alcohol (PVA)-calcium alginate beads (CAPABs). In a typical PVA-calcium alginate bead preparation, two separate 100 mL solutions, one containing mixture of 4 % (w/w) of sodium alginate and 4 % (w/w) of PVA (VWR International ltd, UK) and the other containing mixture of 4 % (w/w) of calcium chloride and (5 % w/w) of boric acid (VWR International ltd, UK), were prepared in pure wate. The resulting beads were isolated, purified and stored as with CABs.

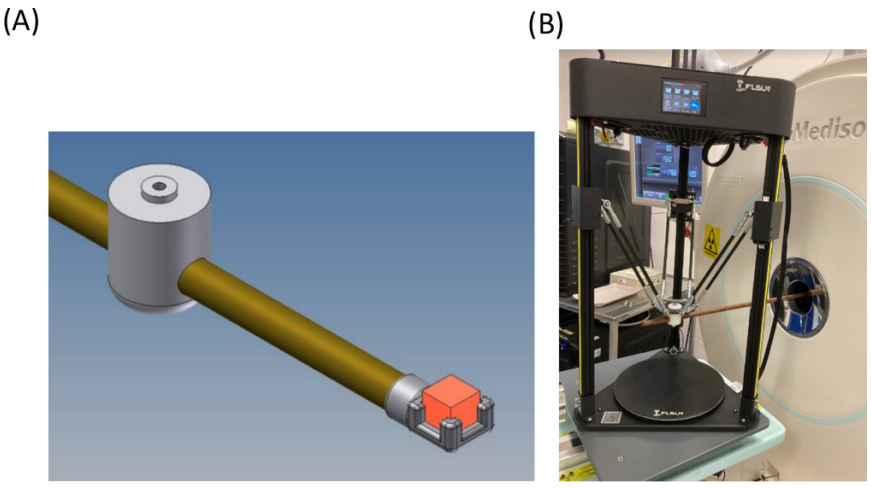

Fig. 2. (A) Modified rod attachment for the 3D printer, (B) Picture of the experimental setup.

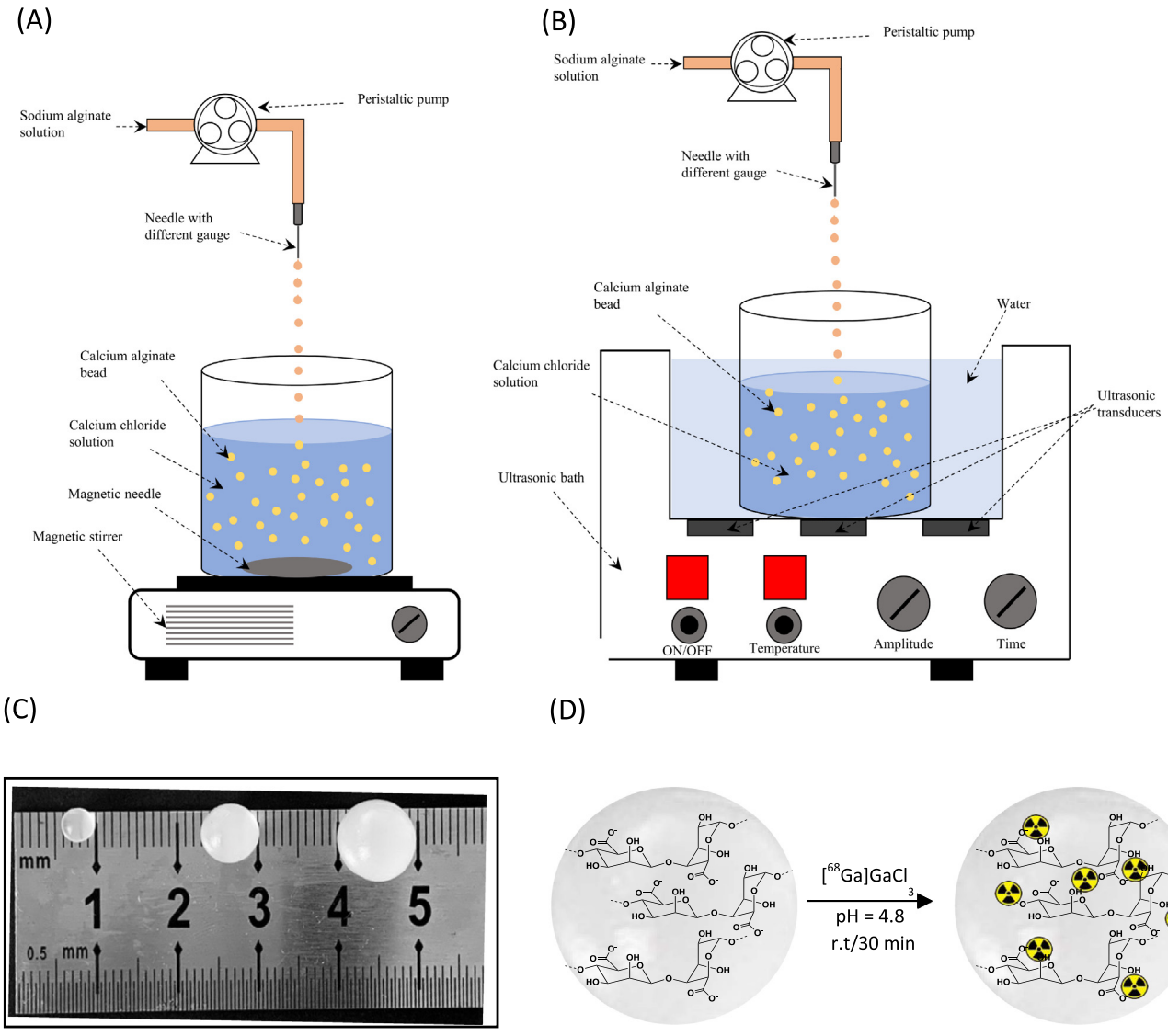

Fig. 3. (A) Schematic representation of the preparation of calcium alginate beads by extrusion dripping, (B) Schematic representation of the preparation of calcium alginate beads by extrusion dripping under ultrasonic irradiation, (C) Visual representation of 4-, 8- and 10-mm calcium alginate beads on the scale, (D) Schematic representation and conditions for the radiolabelling of the beads with ^{68}Ga through the alginate forming the beads.

Table 1
Composition, concentration, and size of the different types of alginate beads used in this study.

Bead	Composition				Bead diameter (mm)
	Solution 1	Concentration (w/w%)	Solution 2	Concentration (w/w%)	
CABs	sodium alginate	4	calcium chloride	4	4, 8,10
	sodium alginate	10	calcium chloride	10	4
10 %-US	sodium alginate	10	calcium chloride	10	4
CASiBs	sodium alginate	4	calcium chloride	4	4
	silica powder	10			
CAPABs	sodium alginate	4	calcium chloride	4	4
	PVA	4	boric acid	5	4

Elution and concentration of [^{68}Ga]GaCl$_3$. Gallium-68 was eluted as [^{68}Ga]GaCl$_3$ from an Eckert and Ziegler ^{68}Ge/^{68}Ga generator in ultrapure 0.1 M HCl (4 mL). The eluate was loaded onto a cation exchange resin Strata-XC column. The cartridge was then washed with 5 mL of a mixture containing acetone/0.1 M HCl (80:20) and dried with air for 20 s. Finally, the cartridge was rinsed with 700 µL of an acetone/0.05 M HCl (98:2) solution, the concentrated [^{68}Ga]GaCl$_3$ collected dried under a N_2 stream and resuspended in 500 µL of 0.5 M HEPES pH = 4.8.

Radiolabelling of alginate Beads with ^{68}GaCl$_3$. The resuspended [^{68}Ga]GaCl$_3$ solution was added over the alginate beads suspended in 500 µL of 0.5 M HEPES pH = 4.8. The mixture was incubated at room temperature for 30 min under stirring. Afterwards, the beads were isolated and washed 5 times with water (5 × 1 mL) to remove unreacted radionuclide. Finally, the radioactivity in the beads and in the washings was measured, and the radiolabelling yield calculated as:

$$\%\mathrm{RLY} = \frac{Activity\ in\ the\ bead/s}{(Activity\ in\ the\ bead/s + Activity\ in\ the\ washings/s)} x100 \quad (1)$$

Radiochemical Stability. To study the stability of the radiolabelling, the bead/s were incubated with water under high stirring for 5, 10, 15, 30, 60 and 120 min. After this time, the bead/s were isolated and washed with water three times and the radioactivity of the bead/s and washings measured. The radiochemical stability was calculated as:

$$\%\mathrm{RCS} = \frac{Activity\ in\ the\ bead/s}{(Activity\ in\ the\ bead/s + Activity\ in\ the\ washings/s)} x100 \quad (2)$$

Phantom PEPT imaging. As an experimental setup, a FLSUN Q5 delta 3D printer was modified by replacing the printer head with a rod attachment used as a robotic arm bearing a holder for an Eppendorf tube (Fig. 2(A)). One radiolabelled ^{68}Ga-CASiB (5.5 MBq) of 4 mm diameter was placed in an Eppendorf, and positioned in the experimental apparatus, in the middle of the scanner's FOV, as pictured in Fig. 2(B). A cubic trajectory of side 1 cm was programmed in G-code. The movement was made to stop for 30 s each time a corner was reached, before resuming. The PET images were acquired whilst the bead was following the programmed trajectory in fine timestamp mode, during an 8-minute-long scan. The listmode file data was extracted from the PET scanner using a MATLAB executable program. PEPT anaylsis was implemented in Python (version 3.8) within PyCharm Community Edition 2021.3.1; (https://www.python.org/) the Birmingham method was used to reconstruct the particle trajectories. A number of algorithms have been developed to reconstruct particle trajectories; the Birmingham method is the most widely used PEPT algorithm and operates by iteratively removing false coincidences from PET data to find the particle position (full details can be found elsewhere) (Parker et al., 1993). The following parameters were used for reconstruction: F_{opt} = 0.5; N = 30000 and N = 50000 (N = number of time-consecutive LORs from full PEPT data). These parameters were chosen based on previous literature and a finite grid search methodology to yield reconstructions that enabled clear visualisation of the particle motion at the different speeds (see Discussion for further explanation) (Parker et al., 1993). The reconstruction algorithm was run on a Surface Pro 6 with an Intel i5 processor and 8 GB RAM.

Statistical analysis. Statistical analyses were carried out by either one-way ANOVA in case of multiple comparisons between more than two samples/conditions or by two-tailed *t*-test for comparison between two samples/conditions. Results are considered to be statistically significant for P < 0.05, *, P < 0.01, **, P < 0.001, ***, and P < 0.0001, ****.

3. Results & Discussion

Calcium alginate beads (CABs) are typically produced by extrusion dripping (Lee et al., 2013). Here, we employed a setting as illustrated in Fig. 3A, where droplets of a sodium alginate solution are deposited over a solution of calcium chloride in a controlled manner. Briefly, a sodium alginate solution is passed through a tube attached to a needle generating a pendant-shaped droplet at the tip of the needle. The pendant droplet grows at the tip of the needle separating from the tip due to gravitational force when the maximum volume is reached. Then, the droplet of the alginate solution hits the surface of the calcium chloride solution experiencing a high deformation and detachment from the liquid–air interface at the surface of the calcium chloride solution. Due to the surface tension and gelation process, the droplet is deformed again taking some time to regain its spherical shape, resulting in monodispersed CABs. To increase the specific surface of the alginate beads, an extrusion drip process was carried out under ultrasound irradiation (Fig. 3(B)). Ultrasonic cavitation involves the formation and collapse of cavities (bubbles) within a short period of time. These cavities collapse asymmetrically, generating a violent shock wave and high-speed jet. The application of ultrasounds during the synthesis of the beads has been reported to produce corrugated microstructures in the rougher surface of the beads, which could potentially provide a high specific surface area available for the attachment of ^{68}Ga (Simonescu et al., 2020).

In general, the properties of the bead are determined by properties of the alginate and calcium chloride solutions, such as surface tension and viscosity. The composition of the beads has been previously reported confirming the presence of higher alginate concentration for beads produced from higher concentrated sodium alginate solutions. Furthermore, the variability in alginate concentration has no significant influence over the bead size (Liu et al., 2002; Ching et al., 2017). In this regard, the diameter of the CABs is approximately twice that of the inner diameter of the needle which permit a fine control over the particle size, a finding that was exploited in this work to prepare beads with different sizes as showed in Fig. 3(C).

Calcium alginate beads (CABs) of 4 mm size were used as reference for further evaluation. After the synthesis of the beads, the radiolabelling reactions were conducted under mild conditions (Fig. 3(D)). First, the ^{68}Ga elution was concentrated using a cation exchange resin as previously reported (Ocak et al., 2010). With this method, the whole elution volume from the ^{68}Ge/^{68}Ga generator, usually 5 mL, is concentrated and resuspended in a desired volume, in this case, 500 μL of a 0.5 M HEPES buffer at pH = 4.8. Then, the CABs were incubated with the ^{68}Ga at room temperature for 30 min and washed for purification to provide the ^{68}Ga radiolabelled CABs (^{68}Ga-CABs). To evaluate the maximum radioactivity per particle, and the effect of the number of beads in the radiolabelling yield (RLY, Eq. (1)), we performed the reaction using different numbers of beads. The RLY increased from 5.9 ± 0.3 for 1 bead to 46.4 ± 2.8 for 10 beads (Fig. 4(A)). This was an expected result since a greater number of beads offers an increased amount of alginate and thus, higher carboxyl/hydroxyl groups for ^{68}Ga coordination. However, the increase in the RLY does not have a significant influence in the specific activity (final amount of radioactivity per bead) with 4.8 ± 0.3 MBq/bead after the radiolabelling of 1 bead and 5.9 ± 0.9 MBq/bead after the radiolabelling of 10 beads (Fig. 4(B)). This result indicate that CABs of this size range have a large capacity to bind ^{68}Ga ions at this concentration.

The radiochemical stability (RCS, Eq. (2)) of ^{68}Ga-CABs was also evaluated, as it provides a direct measurement for the capacity of the radionuclide to stay bound to the material in the medium where the PEPT tracers are going to be used. In our case, the RCS of the ^{68}Ga-CABs was studied for 2 h under heavy stirring in 1 mL of water per bead at room temperature. After this time, the beads were washed 3 times and the radioactivity in the beads compared with the radioactivity in the 1 mL of water and the washings. If the binding between the ^{68}Ga and the CABs is stable, most of the radioactivity should be attached to the beads. We found that 71 ± 10 % of the initial radioactivity remained bound to the 1 bead sample and 85.6 ± 3.4 % to 10 beads (Fig. 4(C)). These values were deemed as sufficiently high to provide satisfactory results in a PEPT experiments, particularly considering the short half-life of ^{68}Ga.

An important parameter that can be controlled during the synthesis of the CABs is the size of the particle. Although particles of 4 mm are the most common for multiphase flows PEPT studies, CABs of different sizes can also be obtained by changing the inner diameter of the needle/capillary used during the bead formation. On this way, CABs of 8 mm and 10 mm diameter were synthesised and radiolabelled with ^{68}Ga to study the effect of the particle size over the radiochemical properties. Considering that in the previous studies with 4 mm CABs (*vide supra*), we did not find differences in the specific activity or the RCS using different numbers of beads, the radiochemical properties of the 8 and 10 mm ^{68}Ga-CABs were evaluated using a single bead. The radiolabelling yield greatly increased with the size reaching 22.5 ± 4.8 % for the 10 mm size bead (Fig. 5(A)). However, no significant differences were observed between the 8 mm and the 10 mm beads indicating that CABs larger than 8 mm might not provide significant improvements on the radiochemical properties. In terms of specific activity, a higher size of particle brought also associated an increase in the activity per bead with 24.0 ± 9.5 MBq/bead for the 10 mm CABs and 20.8 ± 8. 8 MBq/bead for the 8 mm CABs (Fig. 5(B)) which are optimal for PEPT applications. Furthermore, the radiochemical stability showed similar results with no significant differences observed between the beads of different sizes (Fig. 5(C)). It is worth noting that this RCS is high enough for the application of the 8 mm and 10 mm CABs in PEPT studies.

In order to exploit the maximum radiolabelling capabilities of the CABs, we also decided to explore the effect of the alginate concentration, the specific surface and the composition of the beads in the radiolabelling performance. We hypothesised that a higher alginate concentration should lead to a higher number of coordination centres per bead and hence, higher RCY. To study this, CABs were synthesised with an increased alginate concentration (10 % w/w instead of 4 % w/w). To evaluate the influence of a higher specific surface, some of these 10 % w/w in alginate beads were subjected to an ultrasound treatment as detailed above, in order to generate microstructures that we also hypothesised had the potential to increase the radiolabelling efficiency (10 % US). The results showed a dramatic increase in the %RLY from 5.9 ± 0.3 for the 4 % ^{68}Ga-CABs to 34.2 ± 5.3 for the beads with a 10 % of alginate concentration (Fig. 6(A)). This can be explained by the increased numbers of coordinating groups per bead as a result of the increased concentration. These results correspond to a 4-fold increase of the specific activity from 4.8 ± 0.3 MBq/bead for the 4 % ^{68}Ga-CABs to 18.9 ± 6.1 MBq/bead for 10 % ^{68}Ga-CABs (Fig. 6 (B)). This is particularly convenient for the application of these particles as PEPT tracers where a high radioactivity per particle is highly beneficial and improves the noise to background ratio and time resolution of the technique. The generation of micropores in the beads by ultrasounds (10 % US ^{68}Ga-CABs), on the other hand,

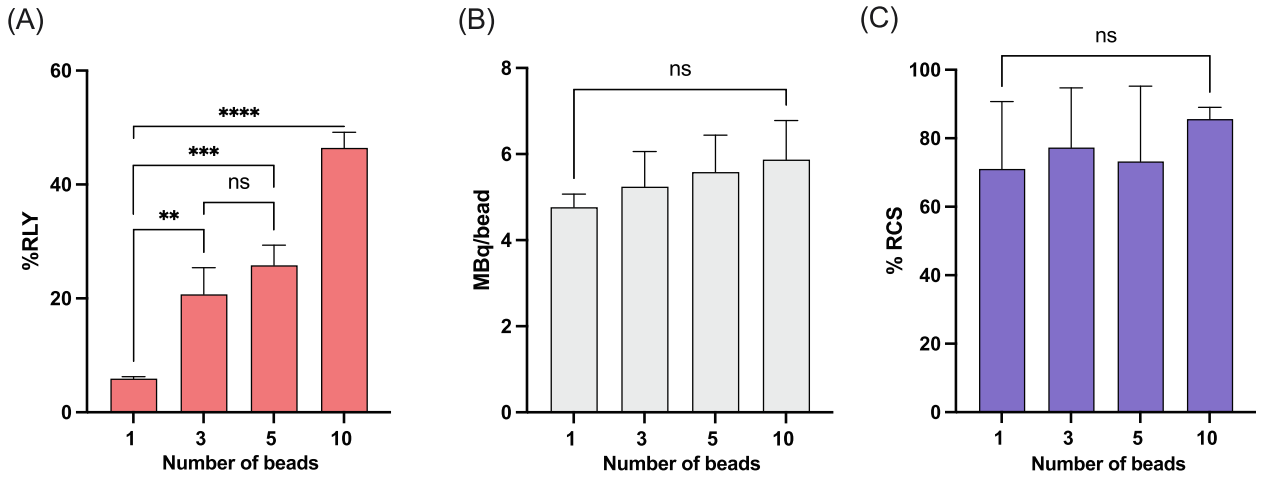

Fig. 4. (A) Radiolabelling yield (RLY) for ^{68}Ga-CABs at different number of beads (ordinary-one-way ANOVA with multiple comparisons,**, p = 0.0023, ***, p = 0.0003 and,****, p < 0.0001). (B) Specific activity in MBq/Bead for ^{68}Ga-CABs at different number of beads (ordinary-one-way ANOVA with multiple comparisons, ns, p greater than 0.05), (C) Radiochemical stability (RCS) of ^{68}Ga-CABs after heavy stirring in water for 2 h (ordinary-one-way ANOVA with multiple comparisons, ns, p greater than 0.05). Data are presented as mean + SD for N = 5.

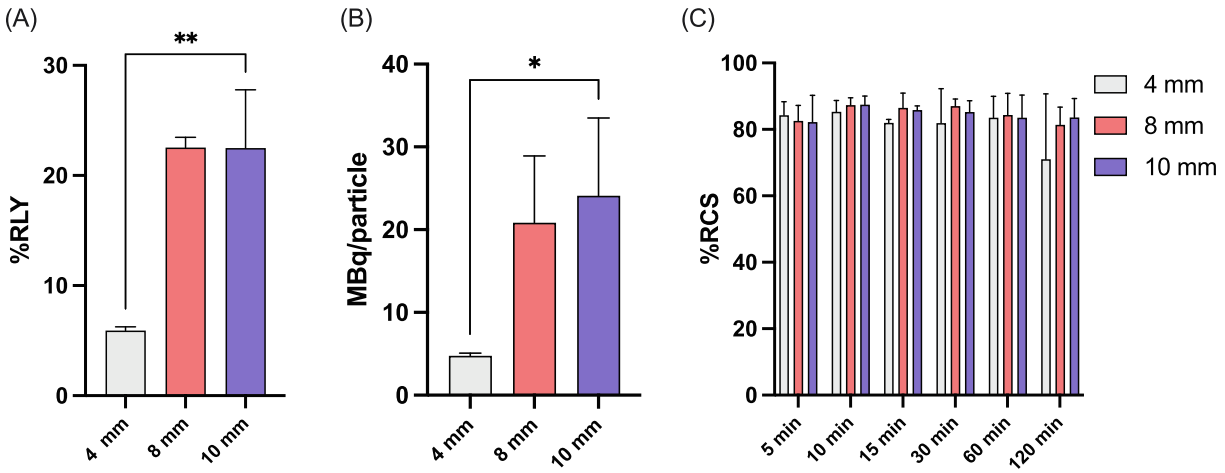

Fig. 5. (A) Radiolabelling yield (RLY) for 4 mm ^{68}Ga-CABs, 8 mm ^{68}Ga-CABs and 10 mm ^{68}Ga-CABs), (two-tailed *t*-test, **, p = 0.0057) (B) Specific activity in MBq/Bead for 4 mm ^{68}Ga-CABs, 8 mm ^{68}Ga-CABs and 10 mm ^{68}Ga-CABs, (two-tailed *t*-test, *, p = 0.023) (C) Radiochemical stability (RCS) of 4 mm ^{68}Ga-CABs, 8 mm ^{68}Ga-CABs and 10 mm ^{68}Ga-CABs after 5 min, 10 min, 15 min, 30 min, 60 min and 120 min under heavy stirring in water. Data are presented as mean + SD for N = 3.

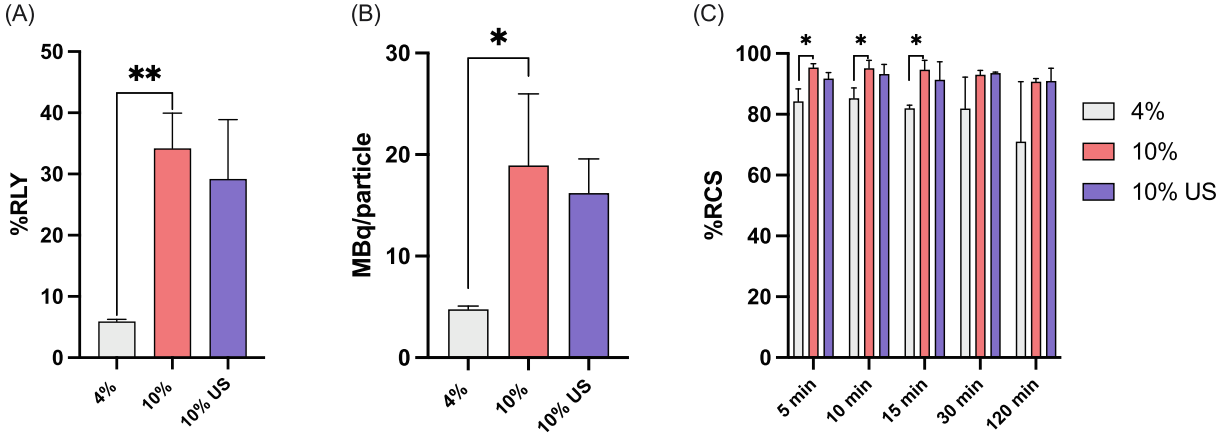

Fig. 6. (A) Radiolabelling yield (RLY) for 4 % ^{68}Ga-CABs, 10 % ^{68}Ga-CABs and 10 % US ^{68}Ga-CABs, (two-tailed *t*-test, **, p = 0.001) (B) Specific activity in MBq/Bead for 4 % ^{68}Ga-CABs, 10 % ^{68}Ga-CABs and 10 % US ^{68}Ga-CABs, (two-tailed *t*-test, *, p = 0.014) (C) Radiochemical stability (RCS) of 4 % ^{68}Ga-CABs, 10 % ^{68}Ga-CABs and 10 % US ^{68}Ga-CABs after 5 min, 10 min, 15 min, 30 min and 120 min under heavy stirring in water, (ordinary-one-way ANOVA with multiple comparisons, *, p < 0.05). Data are presented as mean + SD for N = 3.

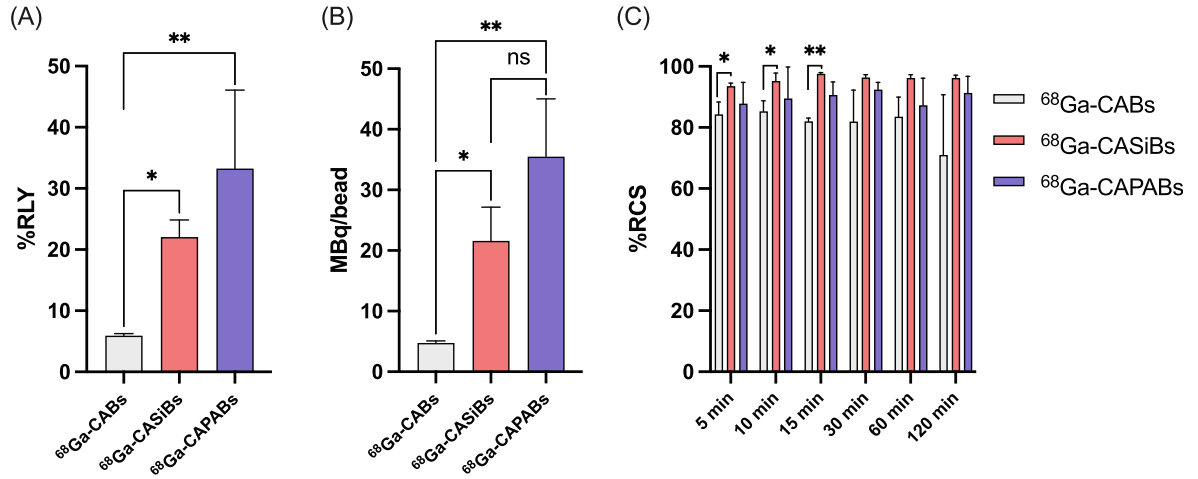

Fig. 7. (A) Radiolabelling yield (RLY) for ^{68}Ga-CABs, ^{68}Ga-CASiBs and ^{68}Ga-CAPABs, (ordinary-one-way ANOVA with multiple comparisons,*, p = 0.026, **, p = 0.0027 and, ns, p = 0.115) (B) Specific activity in MBq/Bead for ^{68}Ga-CABs, ^{68}Ga-CASiBs and ^{68}Ga-CAPABs, (ordinary-one-way ANOVA with multiple comparisons,*, p = 0.040 **, p = 0.0025 and, ns, p = 0.08) (C) Radiochemical stability (RCS) of ^{68}Ga-CABs, ^{68}Ga-CASiBs and ^{68}Ga-CAPABs (N = 3) after 5 min, 10 min, 15 min, 30 min, 60 min and 120 min under heavy stirring in water, (two-tailed *t*-test, *, p < 0.05 and, **, p = 0.001). Data are presented as mean + SD for N = 3.

showed no significant effect on the %RLY or the specific activity. Importantly the increase in alginate concentration also had a beneficial effect on the radiochemical stability in H_2O, with a significant increment on the %RCS for the 10 % and 10 % US ^{68}Ga-CABs (Fig. 6(C)). The values, higher than 90 % for any time point during the first 2 h represent an improvement over the 4 % ^{68}Ga-CABs and the 8–10 mm CABs and confirm the excellent radiochemical properties of the 10 % ^{68}Ga-CABs for PEPT applications. As in the case of the %RLY and the specific activity, no significant changes were observed in the sample subjected to ultrasounds suggesting that a larger specific surface area does not alter the radiochemical properties of the ^{68}Ga-CABs. Overall, the radiochemical properties of the 4 mm CABs with 10 % (w/w) alginate were superior and therefore might be more convenient for PEPT studies depending on the final application.

To study the influence over the particle composition, two different chemical compounds, silica and polyvinyl alcohol (PVA) were used to produce silica encapsulated calcium alginate beads (CASiBs) and PVA encapsulated calcium alginate beads (CAPABs), respectively. These compounds were chosen in order to obtain beads with different densities and hence, expand their applications in multiphase flow studies by PEPT. In addition, silica has been reported to have high affinity and provide stable complexes with ^{68}Ga, which could improve the radiochemical properties of the ^{68}Ga-CABs (Shaffer et al., 2015). After the one-step radiolabelling with ^{68}Ga, the radiochemical properties of the new beads were analysed and compared with the native ^{68}Ga-CABs. By encapsulating silica or PVA the %RLY increased from 5.9 ± 0.3 for ^{68}Ga-CABs to 21.4 ± 3.5 for ^{68}Ga-CASiBs, and 32.3 ± 7.5 for ^{68}Ga-CAPABs (Fig. 7 (A)). This enhancement rendered a dramatic increase in the specific activity with 21.6 ± 5.1 MBq/bead for ^{68}Ga-CASiBs and 35.5 ± 9.5 MBq/bead for ^{68}Ga-CAPABs (Fig. 7(B)). In term of stability, the particles encapsulated with silica demonstrated the best behaviour with values greater than 95 % for the different time points. However, not significant differences between the ^{68}Ga-CABs and the ^{68}Ga-CAPABs were observed (Fig. 7(C)). These results confirm the high specificity of silica towards ^{68}Ga and the poor coordination capabilities of PVA that, although allow a higher incorporation of ^{68}Ga, it is rapidly detached showing no significant stability differences compared to ^{68}Ga-CABs.

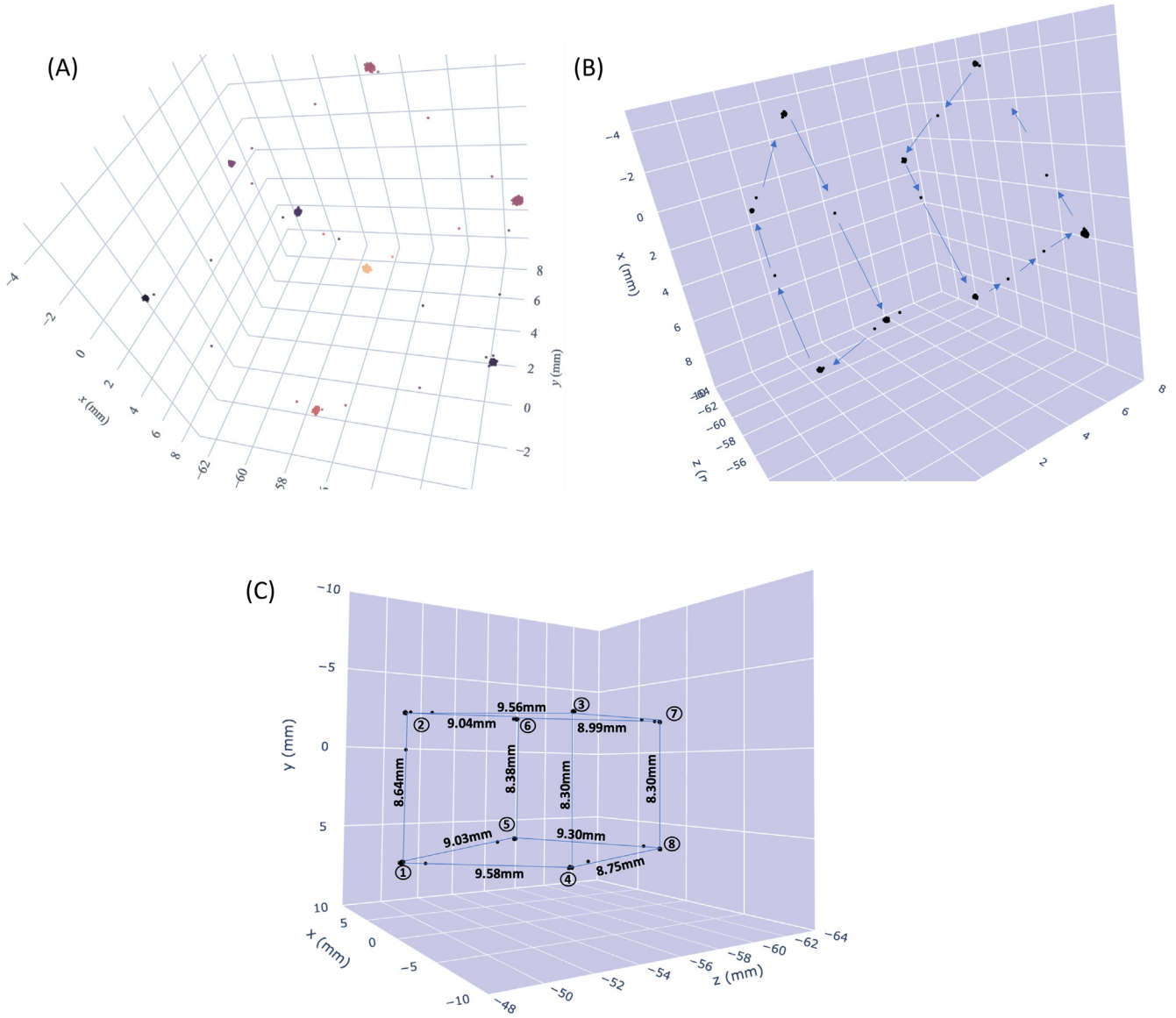

Fig. 8. (A) Reconstructed cube trajectory using N = 30000, (B) Reconstructed cube trajectory using N = 30000 with arrows indicating the trajectory of the bead, (C) Reconstructed cube trajectory using N = 50000 with lines as an aid to the eye, and the distances between points measured (the numbers in the vertices indicate the order of acquisition in the programmed trajectory.

4. PEPT phantom

In order to demonstrate the suitability of the developed beads for PEPT applications, we carried out a phantom acquisition in a NanoPET/CT preclinical scanner. As we aim to track the position of the bead as it moves within the scanner, it is important to control the motion of the particle inside the field of view (FOV) of the scanner with high precision. To achieve this, a modified 3D-printer to hold the radiolabelled bead was employed as described in the materials and methods section (Fig. 2). Among the developed beads, ^{68}GaCASiB were selected as they demonstrated the best radiochemical stability. For the experiment, a single ^{68}GaCASiB (5.5 MBq) was acquired describing a cubic trajectory of a 1 cm side programmed to stop for 30 s in every corner of the cube. The PET data was first reconstructed using a small subset N of lines of response (LoRs) to show the bead being tracked whilst moving between the corners of the cube, as the faster a particle is moving, the smaller number of LoRs required to detect it. From looking at Fig. 8(A), the cubic shape can clearly be discerned, and clusters can be seen in each corner of the cube, as the bead was held stationary in those positions, making them denser in LoRs. Most importantly, singular points can also be seen alongside the spines of the cube, as the bead was moving from one corner to the other hence, tracking the motion of the bead inside the scanner (Fig. 8 (B)). This confirm the properties of the radiolabelled bead for tracking trajectories whilst the particle is moving. Distances between corners could not accurately be determined from this reconstruction, as the N was not enough to determine an accurate spatial error. This was mitigated by reconstructing the data again, this time with a larger subset of LoRs. Spatial accuracy was improved by reconstructing the data again using N = 50000. It was found that the clusters in each corner were much smaller, and that the error in distances varied between 4.2 % and 17 % (Fig. 8(C)). The discrepancies seen here are most likely due to the size of the bead, as our target distance was 10 mm, and the bead was 4 mm in diameter. Nevertheless, the results clearly show that ^{68}Ga-CASIBs can be used to track trajectories with acceptable spatial accuracy. Doubtless this can be further improved with optimisation of the PEPT reconstruction.

5. Conclusions

The applications of PEPT are currently limited to the design of optimal radiolabelled single particle tracers. In this work, calcium alginate beads were produced and explored as potential candidates for the radiolabelling with ^{68}Ga. Using an extrusion dripping method, calcium alginate beads with different particle size, porosity, concentration, and composition were easily synthesised. By incubation under very mild conditions with ^{68}Ga, these particles presented excellent radiochemical properties regardless of the number of beads used for the reaction, the concentration of alginate, the size, or the composition of the bead. Nevertheless, the change on the alginate concentration or the modification with silica or PVA provided a remarkable increase of the specific activities from 4.8 ± 0.3 to 35.5 ± 9.5 MBq per bead. This range of radioactivity is remarkable considering the low initial activity of a ^{68}Ga benchtop generator compared with a cyclotron produced radionuclide and ensures their future successful application in PEPT (Parker, 2017). Most importantly, good radiochemical stabilities were obtained for all the samples from 71 ± 10 % for ^{68}Ga-CABs to the unprecedented values of 96.2 ± 0.9 % for ^{68}Ga-CaSiBs after 120 min. These values guarantee accurate acquisitions in PEPT leading to their employment in high resolution applications. This was corroborated by PEPT phantom experiments demonstrating the ability of the radiolabelled beads to track complex trajectories. In addition, these results represent the first reported example of a ^{68}Ga radiolabelled particle for PEPT. The versatility of the synthesis for the calcium alginate beads in combination with the broad availability of ^{68}Ge/^{68}Ga generators and the straightforward radiolabelling reaction presented here provides an excellent platform to expand the applications of radiolabelled particles for PEPT.

CRediT authorship contribution statement

Juan Pellico: Conceptualization, Methodology, Investigation, Writing - original draft, Writing - review & editing. **Ananda Jadhav:** Methodology, Investigation, Writing – original draft. **Laurence Vass:** Investigation, Validation. **Agathe Bricout:** Investigation, Validation. **Mostafa Barigou:** Supervision. **Paul K. Marsden:** Supervision. **Rafael T.M. de Rosales:** Conceptualization, Supervision, Writing - review & editing.

Data availability

Data will be made available on request.

Declaration of Competing Interest

The authors declare that they have no known competing financial interests or personal relationships that could have appeared to influence the work reported in this paper.

Acknowledgements

The authors wish to thank Professor David Parker (University of Birmingham) for his help with the PEPT phantom. This work was funded by EPSRC programme grants EP/S032789/1 (Probing Multiscale Complex Multiphase Flows with Positrons for Engineering and Biomedical Applications) and EP/R045046/1 (Next Generation Molecular Imaging and Therapy with Radionuclides). We also acknowledge support from the Wellcome/EPSRC Centre for Medical Engineering [WT/203148/Z/16/Z] and the KCL and UCL Comprehensive Cancer Imaging Centre funded by CRUK and EPSRC in association with the MRC and DoH (England). Radioanalytical equipment was funded by a Wellcome Trust Multiuser Equipment Grant: A multiuser radioanalytical facility for molecular imaging and radionuclide therapy research [212885/Z/18/Z]. The authors finally acknowledge support the National Institute for Health Research (NIHR) Biomedical Research Centre based at Guy's and St Thomas' NHS Foundation Trust and KCL [grant number IS-BRC-1215-20006]. The views expressed are those of the authors and not necessarily those of the NHS, the NIHR or the Department of Health. This research was funded in part, by the Wellcome Trust [WT 203148/Z/16/Z][212885/Z/18/Z]. For the purpose of open access, the author has applied a CC BY public copyright licence to any Author Accepted Manuscript version arising from this submission.

References:

Banerjee, S.R., Pomper, M.G., 2013. Appl. Radiat. Isot. 76, 2–13.
Barigou, M., Muller, F.L., 2015. in *Pharmaceutical Blending and Mixing*. Chichester, UK, John Wiley & Sons Ltd, pp. 233–285.
Başağaoğlu, H., Allwein, S., Succi, S., Dixon, H., Carrola, J.T., Stothoff, S., 2013. Microfluid. Nanofluid. 15, 785–796.
Blower, P.J., Cusnir, R., Darwesh, A., Long, N.J., Ma, M.T., Osborne, B.E., Price, T.W., Pellico, J., Reid, G., Southworth, R., Stasiuk, G.J., Terry, S.Y.A., de Rosales, R.T.M., 2021. Adv. Inorg. Chem., 1–35
Ching, S.H., Bansal, N., Bhandari, B., 2017. Crit. Rev. Food Sci. Nutr. 57, 1133–1152.
Cole, K., Buffler, A., Cilliers, J.J., Govender, I., Heng, J.Y.Y., Liu, C., Parker, D.J., Shah, U. V., van Heerden, M., Fan, X., 2014. Powder Technol. 263, 26–30.

Cole, K., Brito-Parada, P.R., Hadler, K., Mesa, D., Neethling, S.J., Norori-McCormac, A. M., Cilliers, J.J., 2022. Chem. Eng. J. 433, 133819.
Fan, X., Parker, D.J., Smith, M.D., 2006. Nucl. Instruments Methods Phys. Res. Sect. A Accel. Spectrometers, Detect. Assoc. Equip., **562**, 345–350.
Hoffmann, A.C., Skorpen, Å., Chang, Y.-F., 2019. Chem. Eng. Sci. 200, 310–319.
Lee, B.-B., Ravindra, P., Chan, E.-S., 2013. Chem. Eng. Technol. 36, 1627–1642.
Liu, X.D., Yu, W.Y., Zhang, Y., Xue, W.M., Yu, W.T., Xiong, Y., Ma, X.J., Chen, Y., Yuan, Q., 2002. J. Microencapsul. 19, 775–782.
McCutchan, E.A., 2012. Nucl. Data Sheets 113, 1735–1870.
Ocak, M., Antretter, M., Knopp, R., Kunkel, F., Petrik, M., Bergisadi, N., Decristoforo, C., 2010. Appl. Radiat. Isot. 68, 297–302.
Parker, D.J., 2017. Rev. Sci. Instrum. 88, 051803.
Parker, D.J., Broadbent, C.J., Fowles, P., Hawkesworth, M.R., McNeil, P., 1993. Nucl. Instruments Methods Phys. Res. Sect. A Accel. Spectrometers, Detect. Assoc. Equip., 1993, **326**, 592–607.
Parker, D.J., Fan, X., 2008. Particuology 6, 16–23.
Shaffer, T.M., Wall, M.A., Harmsen, S., Longo, V.A., Drain, C.M., Kircher, M.F., Grimm, J., 2015. Nano Lett. 15, 864–868.
Shetty, D., Lee, Y.-S., Jeong, J.M., 2010. Nucl. Med. Mol. Imaging 2010 (44), 233–240.
Siddiqui, A.A., Turkyilmazoglu, M., 2019. Micromachines 10, 373.
Siddiqui, A.A., Turkyilmazoglu, M., 2020. Int. Commun. Heat Mass Transf. 113, 104499.
Simonescu, C.M., Mason, T.J., Călinescu, I., Lavric, V., Vînătoru, M., Melinescu, A., Culiță, D.C., 2020. Ultrason. Sonochem. 68, 105191.
Sommer, A.-E., Ortmann, K., Van Heerden, M., Richter, T., Leadbeater, T., Cole, K., Heitkam, S., Brito-Parada, P.R., Eckert, K., 2020. Miner. Eng. 156, 106410.
Tripathi, J., Vasu, B., Subba Reddy Gorla, R., Chamkha, A.J., Murthy, P.V.S.N., Anwar Bég, O., 2021. J. Nanofluids, **10**, 1–30.
Windows-Yule, C.R.K., Seville, J.P.K., Ingram, A., Parker, D.J., 2020. Annu. Rev. Chem. Biomol. Eng. 11, 367–396.
Windows-Yule, C.R.K., Herald, M.T., Nicuşan, A.L., Wiggins, C.S., Pratx, G., Manger, S., Odo, A.E., Leadbeater, T., Pellico, J., de Rosales, R.T.M., Renaud, A., Govender, I., Carasik, L.B., Ruggles, A.E., Kokalova-Wheldon, T., Seville, J.P.K., Parker, D.J., 2022. Rep. Prog. Phys. 85, 016101.